Analysis of 3D Biocompatible Additive Structures Using COMSOL Multiphysics®

E. Lacatus[1*], M.A.Sopronyi[2], G.C. Alecu[1], A. Tudor[1]
[1]Polytechnic University of Bucharest, Romania, [2] INFLPR -National Institute for Laser Plasma and Radiation Physics, Bucharest, Romania

* Assoc. Prof. E. Lacatus, UPB-IMST, 313 Splaiul Independentei , RO-060032; Email: elena.lacatus@upb.ro

Abstract: For biocompatible prosthetics, from dental implants up to bone parts, manufacturers have to find the best way to correlate process parameters and the material properties as to meet the unique needs of individuals.

Additive manufacturing techniques aim at creating complex biocompatible structures able to overcome the present shortfalls of the metal and metal alloys implants related to cytotoxicity, corrosion or stress shielding effects.

Although presently the metallic biomaterials cannot be replaced by ceramics or polymers, the nowadays Selective Laser Sintering technique used for rapid prototyping of these materials can be applied as well for metal powder sintering.

Thus, Direct Metal Laser Sintering (DMLS) was considered for studying the influence of thermal stress during the layer-by-layer sintering process of metal alloy powder and on the thermally induced warping of the dried layers.

Keywords: biocompatible, Marangoni effect, DMLS, heat transfer, FEA

1. Introduction

Equally answering material strengths and biological compatibility requirements additive structures manufactured from powder grains are more likely to become the next patient specific implant material. Although using different additive manufacturing techniques bone substitutes and 3D scaffolds for the growth of advanced biostructures could be the structural applications towards properly personalized medical parts and devices.

Additive manufacturing techniques become more attractive as the technological path downsizes to micro- and even nanosize interface phenomena. Inside the micro sized powder layer complex packaging pressure and heat transfer phenomena are occurring. However, during the layer-wise shaping and material consolidation processes a series of quality drawbacks can occur. The melted, respectively dried powder layer may contain post-processing adherent grains. Gas porosity appears as gas is trapped within powder particles from the shielding gas during processing. Consequently, process parameters must be adjusted in order to obtain adequate densifications of 3D manufactured parts. Layer additive processes are under stair-stepping effect [1], thus non-horizontal part surfaces become rough as a consequence of the slice/slide process occurring during the layer by layer growth. The stair-stepping effect decreases as the slice thickness is reduced but two limits are to be considered: grain size distribution and process efficiency.

2. Theory

Direct Metal Laser Sintering (DMLS) process involves different physical phenomena inside the metal powder grains and on their surface:

a. *Laser beam absorption:* melting, heat transfer, radiation;
b. *Fluid flow*: gravity, wetting, Marangoni convection;
c. *Powder packing*: sintering;
d. *Melted powder*: previous layer solidification;
e. *Unmelted powder*: heat transfer

The strong relationships existing between these physical mechanisms are directly influencing the properties of the processed material.
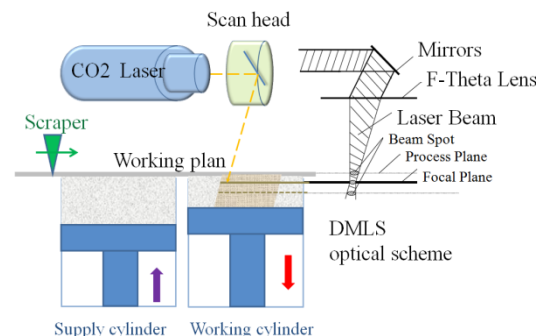

Figure 1. Equipment and method for DMLS process

The schematic DMLS process-flow stages are shown in Figure 6-9. When the laser scans the powder surface, the local temperature increases rapidly, exceeding the melting temperature T_m of the low-melting-point binder but does not reach the melting point of the high-melting point metallic powder.
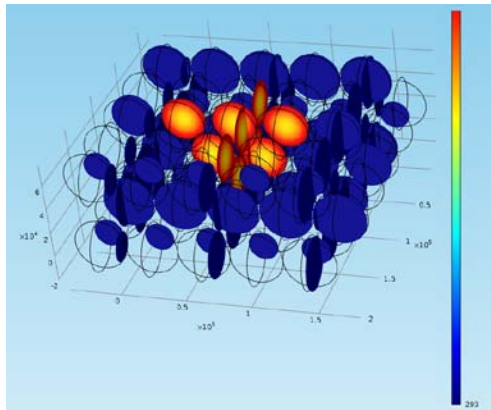

Figure 2. Volume delimited inside powder bed

Rapidly absorbing the laser energy, the binder changes to liquid phase and the metal alloy grain powders that have a high-melting-point remain solid as a structural skeleton during the sintering. Under the force of gravity and capillary (Marangoni effect), the flowing liquid infiltrates into the original atmosphere pores in the raw powder bed [8].
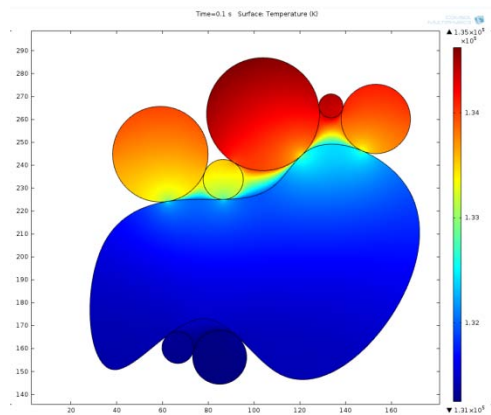

Figure 3. Volume delimited inside powder bed

Thus the part density increases with the shrinkage of the pores and the porosity decreases while the solid grain particles are wetted by the flowing liquid and connected together. On the

following cooling stage, the liquid metallic re-solidifies and binds the solid particles effectively.

Because the time of sintering is short (~0.1s) and the heating /cooling rates are very fast it is difficult to achieve the full density parts (best value 95%) [4,5,9].

It could be problematic for a liquid metal wetting its solid form, especially when the solid has almost the same temperature, thus driving no forces for wetting. A good wetting is critical to the final sintered parts quality but at the same time the viscosity of the liquid hinders the flowing process [3,7].

Consequently, the DMLS processing parameters (laser power, scan speed, hatch distance, thickness, and scan path) have to be chosen to ensure that enough remelting of the previous layer takes place as to maintain the continuity of the solid-liquid interface under the moving beam [6].

2. Governing Equations

The laser beam, used in the DMLS system, may be approximated by a Gaussian function. For a Gaussian laser, the energy intensity (W/m^2) at any point is given by Equation 1 [10]:

$$I(r) = I_0 \exp\left[-\frac{2r^2}{w_0^2}\right] \qquad (1)$$

where: I_0 is energy intensity in the center point of the laser beam, r is the distance from the point to the center, w_0 is the distance in which the laser energy equals to 1/e of I_0, and e is the base of natural logarithms.

In the study of DMLS system, the standard value of w_0 is 0.4mm [3]. I_0 can be calculated based on the laser power P (W) by Equation 2:

$$I(r) = \left[\frac{2P}{\pi w_0^2}\right] exp\left(-\frac{2r^2}{w_0^2}\right) \qquad (2)$$

In the operating situation, the moving laser source with a fixed scan value v scans the powder surface according to the defined scan pattern. Within the powder bed there is a thermal "zone of influence" (Fig.2,3) where a differential area $dA=dxdy$ receives 99.99% of the total radiation [11]. The radius of this zone of influence (R) [4] is considered to be as in Equation 3:

$$R = 2.146 \, w_0 \tag{3}$$

The surface irradiation equation at any point with the y value to the scan line is expressed by Equation 4:

$$E_{(y,0)} = \frac{\sqrt{2} \, P/w_0 S_{scan}}{\pi} \, exp\left(-2y^2/w_0^2\right) \tag{4}$$

where S_{scan} is the scanning speed.

Only part of the laser exposure energy absorbed by the powder system and others are reflected or transmitted by the powder bed. The actual energy absorbed by the powder can be calculated as in Equation 5 [7]:

$$E_{absorb} = \alpha_R E \tag{5}$$

where the fraction absorbed α_R is called the absorptivity, being dependent on the material characteristics, temperature, etc

The time for the powder to absorb the laser energy (99.99%) can be calculated as in Equation 6 [5]:

$$t_{eff} = \frac{\sqrt{R^2 - y^2}}{S_{scan}} \tag{6}$$

Thus for a default S_{scan} of 100mm/s the effective sintering time of each hatch line is less than 10ms. The high sintering rate makes the temperature of the sintered powder increase rapidly.

For the temporary emerging fluid phase, wetting, capillarity and Marangoni effect the laminar flow Equation 7 was considered [7]:

$$\rho(u \cdot \nabla)u = \nabla \cdot [-pI + \mu(\nabla u + (\nabla u)^T)] + F \tag{7}$$

where ρ is density [kg/m^3], u represents dynamic viscosity [Pas], T is temperature [K] and F is volume force [N/m^3]

3. Use of COMSOL Multiphysics

Based on Marangoni effect the Lattice Boltzmann Method (LBM) was used for modelling the interface dynamics during the

interaction of different viscosity droplets. Different process parameters and material properties were considered for this analyses and simulations.

The 2D SolidWorks® models of the grain powder bed (Figure 2, 7, 9, and 13) were imported through LiveLink™ in COMSOL Multiphysics®. The vector structure of the melting powder grains (Figure 3) were imported as well through LiveLink™ module in COMSOL Multiphysics®, considering on the model description the influence of powder grains sizes and their density of distribution on air.

The SolidWorks® model was exported through the LiveLink™ for SolidWorks® add-on in COMSOL Multiphysics® where heat transfer and phase transformation analyses were performed using Marangoni convection model.

4. Methods

Considering a volume unit inside the metal grains powder bed during the DMLS scanning process (Figure 4, 5, 6), the laser beam would be focused on a depth of 100µm below the powder bed surface (Figure 1). This model considers all grains having the same shape and size, and the powder bed having an ideally uniform distribution of the grains. The first two layers below the laser focal plane are considered completely filled with Titanium alloy, for the others air is considered filling the gaps between solid grains.
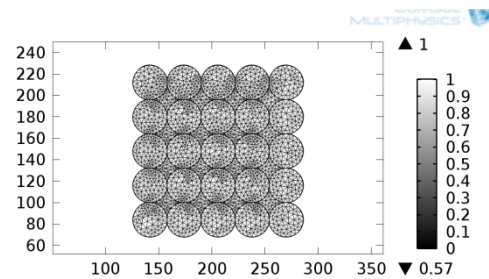

Figure 4. Volume unit inside the powder bed

For Titanium alloy (reaching temperatures for exhibiting Ti(β) phase) heat capacity at constant pressure was Cp=710 [J/kg*K], density ρ=4940 [kg/m^3] and thermal conductivity κ = 7.5 [W/m*K]. Using Heat Transfer in Solids module of COMSOL Multiphysics® not only interesting contour heat fluxes were obtained (Figure 5) but

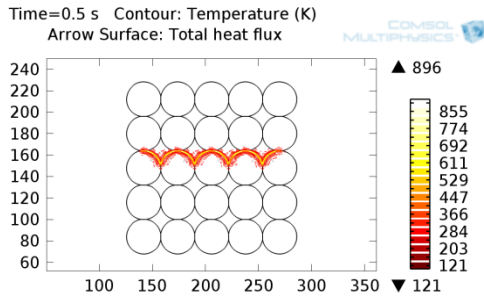as well peak values distributions similar to the experimental models (Figure 6)

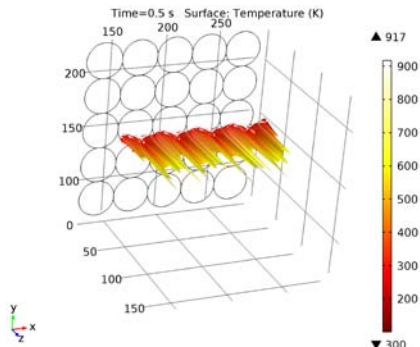**Figure 5.** DMLS power inside the powder bed

Figure 6. Thermal radiation peaks emerging from the powder bed

As the laser beam is absorbed in the powder bed, the powder starts to heat, or even melt, and the volume reduces. Changes of the viscosity between the liquid and solid phase temperature may influence the tracks and the resulting dried surface roughness, leading towards the development of stochastic melt tracks with irregular, corrugated appearance [1].
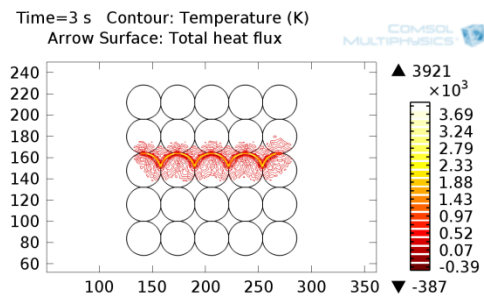

Figure 7. Remelting the dried layer at the solid-liquid interface under the moving DMLS beam

Figure 7 represents the thermal evolution across the remelted layer during the laser scanning. But the dried-remelted layer geometry is far beyond the regular network structure (Figure 2, 4, 5, 7) due to the variation of the effective powder grain size and of the previously corrugated dried layers.

5. Numerical Model

Although the analysis refers to a 3D additive manufacturing technique the models used for the system were 2D cross sections of the unit volume . The parameters used for finite element simulation (FEA) are mentioned in Appendix (Tables 1 to 4).
From Equation 1, I - the intensity of laser beam energy was approximated by a Gaussian function as follows:

$$I=I0*Gauss\_time(t)*Gauss\_space(r) \qquad (8)$$

where: *Gauss_time* and *Gauss_space* are analytical functions defined in the *global definitions* as :

$$Gaus\_time = exp(-3.5((t-tau\_m)*(t-tau\_m))/(tau\_m*tau\_m)) \qquad (9)$$

$$Gauss\_space = exp(-(r^2/r0^2)) \qquad (10)$$

The radius of the laser thermally influenced zone (Figure 1, 2, 6.7.8) from Equation 3 was written as :

$$R= sqrt(2*r^2) \qquad (11)$$

For the fluid phase the laminar flow was described by Equation 7 using the parameters form Table 1 (Appendix) and the variables from Table 2 on COMSOL Multiphysics®
Using the model equations of COMSOL Multiphysics® Tutorial –*Marangoni convection* a more realistic approach on the successive heat transfer on the powder bed active layer during successive sintering was obtained, including wetting, melting and flowing variables. Thus, for the volume force F (Equation 7), considering the related data from Table 1-5 and the numerical values F(x,y) is $F_x=0$ and F_y becomes :

$$F=rho1*(g\_const)* alpha1*(T-T\_ref) \qquad (12)$$

where : $rho1$=4110 [kg/m3] represents the density of melted Titanium alloy, $alpha1$=1.14x10^{-4}[1/K] is the thermal expansion coefficient for melted Titanium alloy $T\_ref=T_{ref}$ data were selected from the running model [K] g_const =9.8 [m/s^2] is the value of gravitational acceleration

6. Experimental Results

For a more realistic analysis of the relationships existing between wettability, particle sizes and their position within the dried layer the latest powder layer was removed from figure 5 .
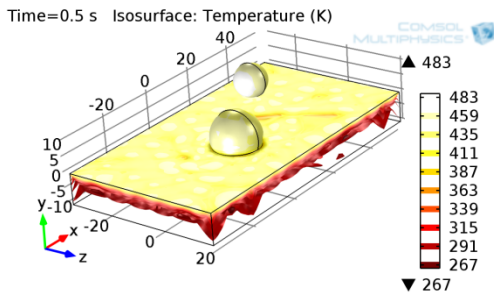

Figure 8. Isosurface temperature for controlled roughness model active layer (t=0.5s)

Running numerical models having only two partially melted grains on the active layer surface (which would be partially remelted during the next scanning phase of DMLS) important heat transfer data were observed. The temporary shape and uniformity of the intermediate layer influences firstly the distribution of the density of energy on the contact surface and afterwards the wettability, adherence and stability of the grains coming on a successive layer.
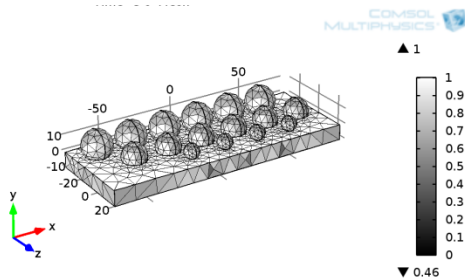

Figure 9. Mesh structure for controlled pattern rough active layer

Extending these findings on a more roughness but still organized active layer surface a new model was created (Figure 9, 10), introducing within the model all the other process variables (gravity, capillarity, Marangoni effect, wettability, etc).
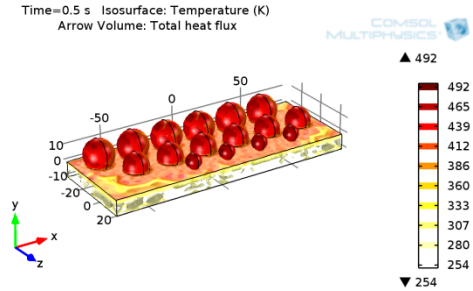

Figure 10. Isosurface temperature for controlled pattern rough active layer (t=0.5s)

Heat conduction as a function of laser scanning time and directivity was suggestively illustrated (Figure 11) using Marangoni convection in COMSOL Multiphysics®.
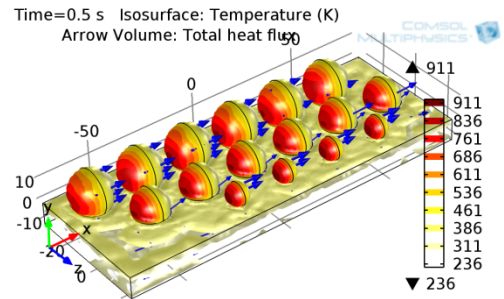

Figure 11. Marangoni convection-heat flow for controlled pattern rough active layer (t=0.5s)
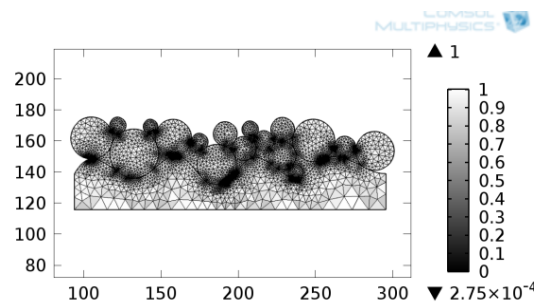
7. Results

Figure 12. Mesh structure for rough active layer

For the powder bed formed with particles with different sizes a rain model packing algorithm was used to describe the generation of successive layers. Thus it was assumed that a falling particle reaching a stationary one was following a rolling round trajectory around the stationary particle aiming to minimize its vertical coordinate.
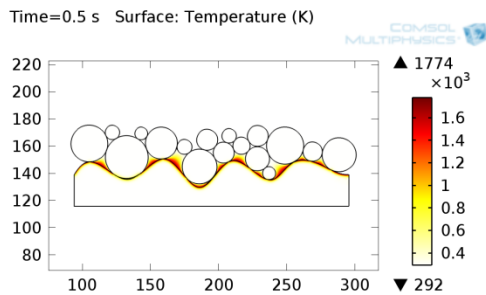

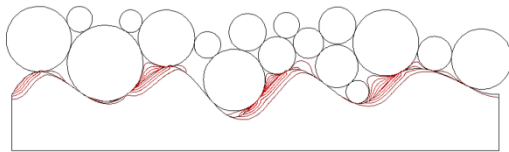**Figure 13.** Temperature distribution on rough active layer (t=0.5s)

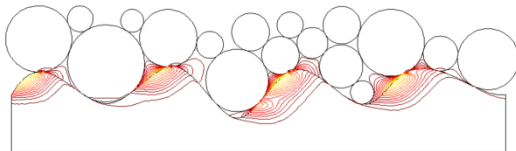**Figure 14.** Contour: Temperature (K) Arrow Surface: Total heat flux (t=0.5s, T=[0.35-0.97]x10^4)

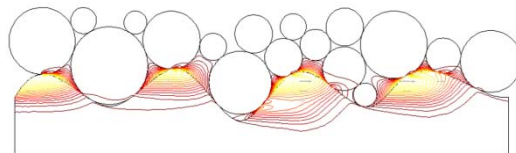**Figure15.** Contour: Temperature (K) Arrow Surface: Total heat flux (t=1.5s, T=[0.25-1.67]x10^4)

Figure 16. Contour: Temperature (K) Arrow Surface: Total heat flux (t=3s, T=[0.17-1.97]x10^4)

Each phase of the process was properly described and designed with the use of 3D/2D plot groups and line graph tools in COMSOL Multiphysics®. The step by step analyses were considered using process related increments. During the validation phase the 2D model accurately predicted the main characteristics of the experiments for each of the 3D additive layer wise shaping method analyzed.

.

8. Conclusions

Using the COMSOL Multiphysics® analysis and simulations a new path of energy distribution and soldering geometry   was designed and modelled for 3D additive growth of biocompatible substances with impact on personalized medicine.

9. References

1. Agawals, M.K., et al., Direct selective laser sintering of metals. Rapid Prototyping Journal, Volume 1, Number 1, pp.26-36. (1995)
2. Asgharzadeh H., Simchi A., Effect of sintering atmosphere and carbon content on the densification and microstructure of laser-sintered M2 high-speed steel powder, Materials Science and Engineering A 403290–298, (2005)
3. Attar E., Simulation der selektiven Elektronenstrahlschmelzprozesse, Der Technischen Fakultät der Universität Erlangen-Nürnberg zur Erlangung des Grades Doktor – Ingenieur (2011)
4. Berto 1 , Medical design: Direct metal laser sintering of Ti–6Al–4V. J Mater Design doi:10.1016/j.matdes.2010.02.050 ,(2010),
5. Khaing M.W. *et al*, Direct Metal Laser Sintering for Rapid Tooling, Journal of Materials Processing Technology 113 269-272,(2001)
6. Murr L.E. *et al*, Microstructure and Mechanical Behaviour of Ti-6Al-4V, Journal of the Mechanical Behavior of Biomedical Materials 2 20-32, (2009)
7. Niu H. J., Chang I. T. H., Instability of scan tracks of selective laser sintering of high speed steel powder, Scripta Mater. 41 (1) 1229 , (1999)
8. Simchi A. , Pohl H., Effects of laser sintering processing parameters on the microstructure and densification of iron powder, Materials and Engineering A359, 119-128, (2003)
9. Thijs L.,*et al*, A study of the microstructural evolution during selective laser melting of Ti-6Al-4V, Acta Materiala 58, 3303-3312,(2010)
10. Tontowi, A.E. and Childs, T.H.C., Density Prediction of crystalline Polymer Sintered Parts at Various Powder Bed Temperatures (Selective Laser Sintering Case), Rapid Prototyping Journal, Vol.7, No.3, pp.180-184, (2001)
11. Traini T., *et al*, Direct laser metal sintering as a new approach to fabrication of an isoelastic functionally graded material for manufacture of

porous titanium dental implants, Dental Materials, Volume 24, Issue 11, November, Pages 1525-1533,(2008)

12. Ziemian, C. W. and Crawn III, P. M., "Computer aided decision support for fused deposition modeling", Rapid Prototyping Journal, Vol. 7, No. 3, 2001, pp.138-147, (2001)

10. Appendix

Table 1 Fluid phase metal alloy parameters

Name	Expression	Description
T_right	273.15[K]	Temperature on the right boundary
DeltaT	1e-3[K]	Excess temperature on the left boundary
gamma	-8e-5[N/(m*K)]	Temperature derivative of the surface tension
rho1	760[kg/m^3]	Fluid density
mu1	4.94e-4[Pa*s]	Dynamic viscosity
k1	0.1[W/(m*K)]	Thermal conductivity
Cp1	2090[J/(kg*K)]	Heat capacity

Table 2 Laminar flow variables

Name	Expression	Description
spf.nx	dnx	Normal vector, x component
spf.ny	dny	Normal vector, y component
spf.nz	0	Normal vector, z component
spf.nxmesh	root.dnxmesh	Normal vector (mesh), x component
spf.nymesh	root.dnymesh	Normal vector (mesh), y component
spf.nzmesh	0	Normal vector (mesh), z component
spf.dz	1	Channel thickness

Table 3 Shape Functions for fluid phase

Name	Shape function	Unit	Description	Shape frame
u	Lagrange (Linear)	m/s	Velocity field, x component	Material
v	Lagrange (Linear)	m/s	Velocity field, y component	Material
p	Lagrange (Linear)	Pa	Pressure	Material

Table 4 Weak Expressions for Fluid Phase

Weak expression	Integration frame
(p-spf.K_stress_tensorxx)*test(ux)-spf.K_stress_tensorxy*test(uy)-spf.K_stress_tensoryx*test(vx)+(p-spf.K_stress_tensoryy)*test(vy)	Material
spf.Fx*test(u)+spf.Fy*test(v)-spf.rho*(ux*u+uy*v)*test(u)-spf.rho*(vx*u+vy*v)*test(v)	Material
-spf.rho*spf.divu*test(p)	Material
spf.crosswindns	Material
spf.streamlinens	Material